KSCE Journal of Civil Engineering (2023) 27(6):2477-2485
DOI 10.1007/s12205-023-1677-5

pISSN 1226-7988, eISSN 1976-3808
www.springer.com/12205

Geotechnical Engineering

Influence of Soil Suction and Seismic Excitation on Active Earth Pressure

Long Wang[a,b], **You Gao**[c], **Lei Wang**[d], **Junran Zhang**[e], **and Bo Chen**[b]

[a]*School of Environment and Civil Engineering, Jiangnan University, Wuxi 214122, China*
[b]*College of Civil Engineering and Architecture, Quzhou University, Quzhou 324000, China*
[c]*School of Civil and Environmental Engineering, Ningbo University, Ningbo 315211, China*
[d]*School of Urban Railway Transportation, Shanghai University of Engineering Science, Shanghai 201620, China*
[e]*Henan Province Key Laboratory of Geomechanics and Structural Engineering, North China University of Water Resources and Electric Power, Zhengzhou 450045, China*

ARTICLE HISTORY

Received 14 September 2022
Revised 9 January 2023
Accepted 12 March 2023
Published Online 20 April 2023

KEYWORDS

Active earth pressure
Unsaturated backfill
Limit analysis
Matric suction
Pseudo-dynamic approach

ABSTRACT

Earthquake-induced slope failures are common occurrences in engineering practice. The rigid gravity retaining wall remains an effective technique in maintaining the slope stability. Based on the pseudo-dynamic approach, the seismic response of unsaturated backfills is studied using the kinematic limit analysis method. To formulate the energy balance equation, a horizontal slice method is proposed. The work rates of unsaturated soil gravity, seismic inertia force and damping force that are all characterized with conspicuous nonlinear distribution characteristics are computed using this method. A series of parametric analysis is conducted regarding the influences of soil suction and seismic excitations on the earth pressure estimations. The results show that the suction effect relates not only to the soil types but also the seismic excitations. The earth pressure is overestimated by 15% – 32% when soil suction is not considered in the analyses. For hard backfills, the peak active earth pressure increases slightly and moves towards the negative direction.

1. Introduction

To maintain the stability of earth works, retaining structures, such as rigid gravity retaining walls, are widely used in engineering practice. The stability of these retaining structures relates closely to the pressures exerted by the backfills and therefore a precise estimation of the lateral earth pressures promises a safe and economical design. In recent years, numerous efforts have been made to estimate the active earth pressure in different scenarios (Fathipour et al., 2021; Lei et al., 2021; Zhang and Yang, 2021; Zhang et al., 2022), among which the seismic excitation remains the main factor in triggering the geostructures failures.

The rationality in the seismic load descriptions is crucial in producing satisfactory results. Experimental investigations shown that the pseudo-dynamic approach remains a simple and realistic way to describe the earthquake (Steedman and Zeng, 1990; Zeng and Steedman, 1993). This method bears an advantage over the pseudo-static one in accounting for the time-history related features of the ground motions. Therefore, it is usually combined with the theoretical analysis methods to predict the seismic stability of typical slopes and retaining structures (Qin and Chian, 2019; Fathipour et al., 2021; Kokane et al., 2021; Lei et al., 2021; Zhang and Yang, 2021).

In reality, the soils in nature and in engineering practice are mostly unsaturated. The physical and mechanical properties between saturated and unsaturated soils exhibit conspicuous differences (Bishop, 1959; Fredlund and Morgenstern, 1977; Fredlund and Xing, 1994; Vanapalli et al., 1996; Lu and Likos, 2004; Chen et al., 2021; Wang et al., 2022; Zhou et al., 2022; Chen et al., 2023), resulting in significant difference in slope stability estimations. Because of the complexity in soil suction, producing realistic results on the slope stability becomes extremely elaborated (Scaringi et al., 2018; Sun et al., 2019; Wang et al., 2019; Zhang and Yang, 2021; Hu et al., 2022). In current seismic active earth pressure estimations, however, comprehensive study on the suction effect and the seismic actions has not well documented.

Based on the pseudo-dynamic approach, the seismic active earth pressure of unsaturated backfills is studied using the kinematic limit analysis approach. A horizontal slices method is descripted to formulate the energy balance equation. The work

CORRESPONDENCE Bo Chen chen.bo@qzc.edu.cn College of Civil Engineering and Architecture, Quzhou University, Quzhou 324000, China

rates of unsaturated soil gravity, seismic inertia force and damping force are computed. Typical illustrative slopes are analyzed to demonstrate the suction effect, the seismic response of the unsaturated backfills.

2. Seismic Active Earth Pressure of Unsaturated Backfills

2.1 Strength of Unsaturated Backfills

An backfill with a height of H and an inclination angle of β restrained by rigid gravity retaining wall is studied, as illustrated in Fig. 1. The phreatic water locates underneath the wall toe with a depth of z_0. The backfill is unsaturated and its behavior can be captured satisfactorily using the Mohr-Coulomb failure criteria. Frequently, the improvement in soil strength because of the soil suction is considered as a cohesion value. Vanapalli et al. (1996) proposed an equation to predict the capillary cohesion using the soil water characteristic curve (SWCC) as

$$c_{cap} = \psi\left[\left(\frac{\theta_w-\theta_r}{\theta_s-\theta_r}\right)\tan\phi'\right], \tag{1}$$

in which ψ' is soil friction angle; ψ denotes the matric suction; θ_w represents the volumetric water content; θ_s is saturated volumetric water content; and θ_r is residual volumetric water content. Given the saturated unit soil weight γ_{sat} and the dry unit soil weight γ_d, the volumetric water content at saturated condition can be derived as $\theta_s = (\gamma_{sat}-\gamma_d)/\gamma_w$.

Following Fredlund and Xing (1994), the volumetric water content for unsaturated backfills can be described using the SWCC as

$$\theta_w = \left\{1-\frac{\ln(1+\psi/\psi_r)}{\ln(1+10^6/\psi_r)}\right\}\frac{\theta_s}{\left\{\ln\left[e+(\psi/a_f)^{n_f}\right]\right\}^{m_f}}, \tag{2}$$

where ψ_r denotes the residual matric suction; m_f is a fitting parameter; and n_f is the SWCC gradient at the inflection point; a_f is the matric suction corresponding to the inflection point of the SWCC. Fig. 2 shows the SWCCs for four typical unsaturated soils. Generally, SWCC A and B describe sandy soils and fine-grained soils such as silt. SWCC C and D represent clays and extremely fine-grained soils. For steady flow conditions, the matric suction can be expressed analytically as (Lu and Likos, 2004)

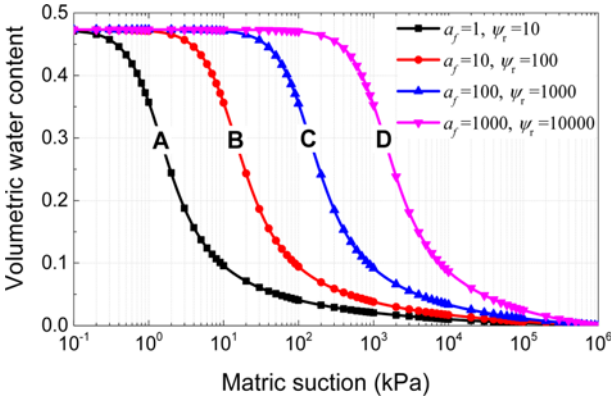

Fig. 2. SWCCs for Four Typical Unsaturated Soils

$$\psi = -\frac{1}{\alpha}\ln\left[(1+q/k_s)\,e^{-\alpha\gamma_w(z+z_0)}-q/k_s\right], \tag{3}$$

where α relates closely to the air-entry pressure; q/k_s is specific discharge; γ_w is unit weight of water; z is the depth measured from the phreatic line; and z_0 is the phreatic line depth. Given the dry unit soil weight, the unit weight of unsaturated backfill is derived as $\gamma' = \gamma_d + \theta_w\gamma_w$.

2.1 Pseudo-Dynamic Approach

The pseudo-dynamic approach can account for the dynamic features of seismic action reasonably by introducing the time. In the seismic wave propagations, the upward waves reflect back to the slope at the backfill surface. This scenario, however, is really

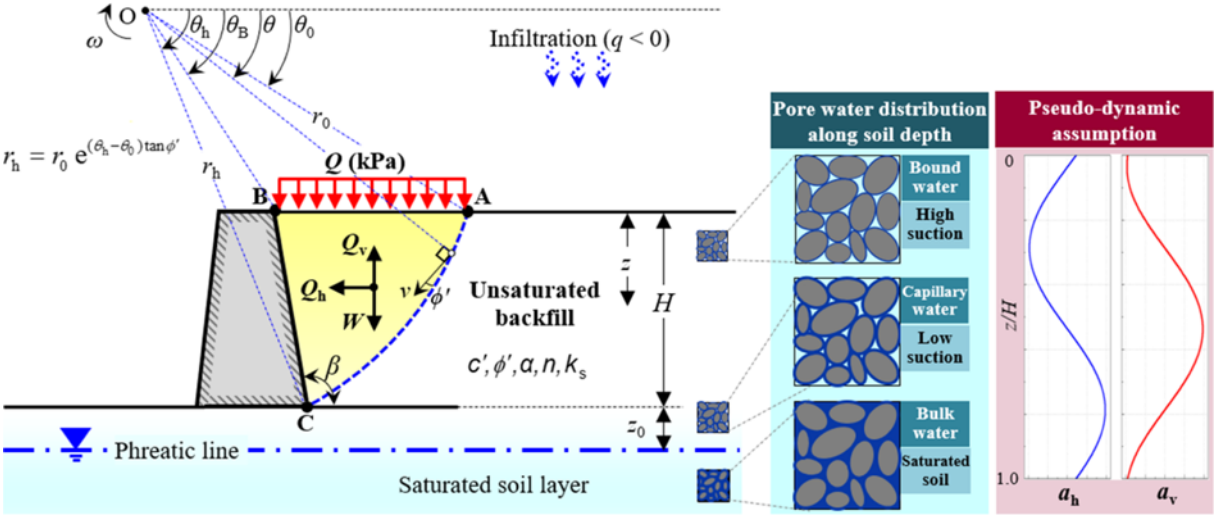

Fig. 1. Diagram of Active Earth Pressure in Unsaturated Backfills Considering the Seismic Loads

elaborated to be accounted for using theoretical approaches. In present analysis, the inertia forces pointing outward and upward the backfill are considered using the pseudo-dynamic assumption, as illustrated in Fig. 1. Validations of this method in seismic active earth pressure estimations have been demonstrated by comparing the theoretical results with the centrifuge model test results (Steedman and Zeng, 1990; Zeng and Steedman, 1993). In this approach, sinusoidal vibrations are used to describe the earthquake waves and a phase shift can be found between the toe and the backfill crest. The horizontal and vertical seismic accelerations can be predicted using the following sinusoidal functions (Steedman and Zeng, 1990; Choudhury and Nimbalkar, 2006)

$$a_h(z_s,t)=k_h g\left[1+(f_a-1)\frac{(H-z_s)}{H}\right]\sin\left[\omega_s\left(t-\frac{H-z_s}{V_s}\right)\right], \quad (4)$$

$$a_v(z_s,t)=k_v g\left[1+(f_a-1)\frac{(H-z_s)}{H}\right]\sin\left[\omega_s\left(t-\frac{H-z_s}{V_p}\right)\right], \quad (5)$$

where V_s and V_p denote shear and primary wave velocities; k_h and k_v represent horizontal and vertical seismic acceleration coefficients; f_a is an amplification factor; z_s is depth measured from the backfill crest; t is time and ω_s is seismic wave angular velocity ($\omega_s = 2\pi/T$ with T being the seismic period).

The shear and primary wave velocities in soils can be estimated empirically with given soil's shear modulus G, density and Poisson's ratio v. For unsaturated backfills, the wave velocities propagate nonlinearly along the soil depth, i.e.,

$$V_s=\sqrt{\frac{Gg}{\gamma_d+\theta_w\gamma_w}}, \quad (6)$$

$$V_p=\sqrt{\frac{G(2-2\nu)g}{(\gamma_d+\theta_w\gamma_w)(1-2\nu)}}. \quad (7)$$

To predict the dynamic responses of geostructures satisfactorily, the damping information is required. Commonly, the Rayleigh damping (Liu and Gorman, 1995) is utilized and can be expressed in two terms of the mass and stiffness matrixes (i.e., $[C]=\alpha_0[M]+\alpha_1[K]$ with α_0 and α_1 being the damping coefficients). It is assumed, in this paper, that the mass and stiffness matrices contribute equally to Rayleigh damping and only the influence of mass matrix is considered. Given the damping ratio ζ and soil natural frequency of vibration ω_n (i.e., the basic frequency of the slope frequency and is postulated to be 1 Hz in this analysis), the coefficient α_0 can be expressed as $\alpha_0 = \zeta\omega_n$.

Given the damping formulation and the corresponding velocity, the damping force can be readily computed. The horizontal and lateral propagation velocities of the soil block $v_h(z_s, t)$ and $v_v(z_s, t)$ can be obtained by integrating the corresponding accelerations, i.e.,

$$v_h(z_s,t)=\frac{(f_aH-f_az_s+z_s)k_hg}{H\omega_s}\left\{\cos\frac{\omega_s(z_s-H)}{V_s}-\cos\frac{\omega_s\left[tV_s+(z_s-H)\right]}{V_s}\right\}, \quad (8)$$

$$v_v(z_s,t)=\frac{(f_aH-f_az_s+z_s)k_vg}{H\omega_s}\left\{\cos\frac{\omega_s(z_s-H)}{V_p}-\cos\frac{\omega_s\left[tV_s+(z_s-H)\right]}{V_p}\right\}. \quad (9)$$

3. A Horizontal Slices Method

3.1 Work Rates by External Forces

To formulate the energy balance equation, a horizontal slices method was proposed to compute the work rate of soil gravity, as illustrated in Fig. 3. The rotational mechanism is discretized by dividing the polar angle into numerous elements equally, i.e., $\Delta\theta = (\theta_h-\theta_0)/m$.

The position of soil layer i can be described by its radius r_n and angle θ_n, i.e.,

$$\theta_n=\theta_0+(i-1)\times\Delta\theta, \quad (10)$$

$$r_n=r_0\exp\left[(i-1)\Delta\theta\tan\phi'\right]. \quad (11)$$

Take per unit width of the rigid wall to calculate and the area of the soil layer can be expressed as

$$S_i=0.5(l_{mn}+l_{m'n'})(r_{n'}\sin\theta_{n'}-r_n\sin\theta_n), \quad (12)$$

where l_{mn} and $l_{m'n'}$ are the length of the upper and bottom surface of this soil layer and can be found from the geometrical and trigonometrical relations as

$$l_{mn}=r_n\cos\theta_n-r_h\cos\theta_h-(r_h\sin\theta_h-r_n\sin\theta_n)\cot\beta, \quad (13)$$

$$l_{m'n'}=r_{n'}\cos\theta_{n'}-r_h\cos\theta_h-(r_h\sin\theta_h-r_{n'}\sin\theta_{n'})\cot\beta. \quad (14)$$

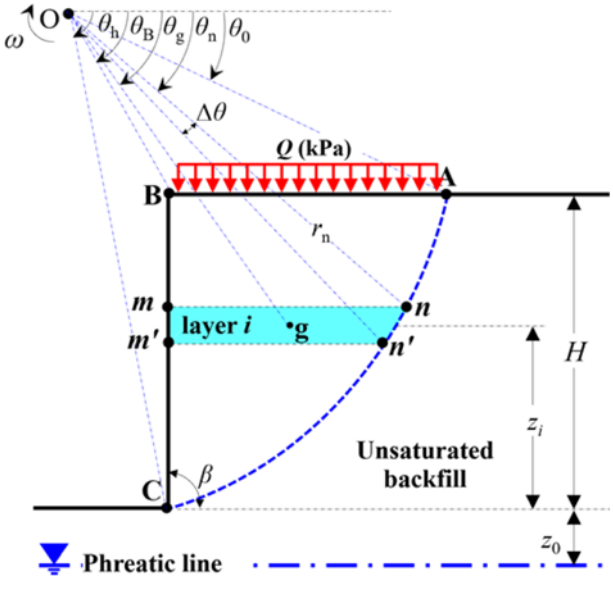

Fig. 3. Diagram of the Horizontal Slices Method to Calculate the Work Rate of Soil Gravity, Seismic Forces and the Work Dissipation Rate of Damping Force

The work rate done by soil gravity in the soil layer can be derived as

$$W_{\gamma'}^{mnn'm'} = S_i\gamma'(z_i)L_g\cos\theta_g\,, \tag{15}$$

where $\gamma'(z_i)$ denotes the unit weight of the soil layer; z_i is the distance measured vertically from the layer centroid to the wall toe; and L_g and θ_g are the radius and angle corresponding to centroid of the soil element and can be found as

$$z_i = r_h\sin\theta_h - r_n\sin\theta_n - 0.5(r_{n'}\sin\theta_{n'} - r_n\sin\theta_n)\,, \tag{16}$$

$$L_g = 0.25\sqrt{(r_n + r_{n'})^2 + 0.25(l_{mn} + l_{m'n'})^2 - (r_n + r_{n'})(l_{mn} + l_{m'n'})\cos\left[0.5(\theta_n + \theta_{n'})\right]}, \tag{17}$$

$$\theta_g = \theta_n + \arcsin\left[(0.5l_{mn}/L_g)\sin\theta_n\right]. \tag{18}$$

The total work rate of soil weight can be written as

$$W_{\gamma'} = \sum_{i=1}^{m} S_i\gamma'(z_i)L_g\cos\theta_g\,. \tag{19}$$

Similarly, the total work rate of horizontal and vertical seismic force can be derived as

$$W_{\mathrm{s}}^{ah} = \sum_{i=1}^{m} a_h\left[t,(H-z_i)\right]S_i\gamma'(z_i)L_g\sin\theta_g \tag{20}$$

$$W_s^{av} = \sum_{i=1}^{m} a_v\left[t,(H-z_i)\right]S_i\gamma'(z_i)L_g\cos\theta_g\,. \tag{21}$$

The static and seismic work rate of the surcharge load on the backfill surface can be derived as

$$W_Q = \omega L_{\mathrm{AB}}Q(r_0\cos\theta_0 - 0.5L_{\mathrm{AB}})\,, \tag{22}$$

$$W_Q^{ah} = \omega L_{\mathrm{AB}}Qa_h(0,t)(r_0\cos\theta_0 - 0.5L_{\mathrm{AB}}) \tag{23}$$

$$W_Q^{av} = \omega r_0 L_{\mathrm{AB}}Qa_v(0,t)\sin\theta_0\,, \tag{24}$$

where L_{AB} denotes the length between points A and B on the backfill surface and can be found from the geometrical relation as

$$L_{\mathrm{AB}} = r_0\cos\theta_0 - \cot\beta H - r_h\cos\theta_h\,. \tag{25}$$

3.2 Internal Work Dissipation Rate

For the assumed log-spiral slip surface, the work rate of energy dissipation along this surface takes the following form as

$$D_c = \omega r_0^2\int_{\theta_0}^{\theta_h}\left[c_{cap}(z_1) + c'\right]\exp 2(\theta-\theta_0)\tan\phi' d\theta\,, \tag{26}$$

where $c_{cap}(z_1)$ is the capillary cohesion corresponding to the layer element; and z_1 denotes the distance measured vertically from the centroid of the soil layer to the ground surface, i.e.,

$$z_1 = r_h\sin\theta_h - r_0\exp\left[(\theta-\theta_0)\tan\phi'\right]\sin\theta\,. \tag{27}$$

The work rate dissipation of damping force in the whole sliding soil mass can be written as

$$D_s^h = \sum_{i=1}^{m}\alpha_0 v_h\left[t,(H-z_i)\right]S_i\rho'(z_i)\,, \tag{28}$$

$$D_s^v = \sum_{i=1}^{m}\alpha_0 v_v\left[t,(H-z_i)\right]S_i\rho'(z_i)\,. \tag{29}$$

3.3 Active Earth Pressure Coefficient

The work dissipation rate of the adhesive force P_{ad} acting on the soil-wall interface can be derived as

$$D_{p_{ad}} = \omega r_0\frac{\tan\delta}{\tan\phi'}\int_0^H\left(c_{cap}(h) + c'\right)\frac{dh}{\sin\beta} \exp\left[(\theta_h-\theta_0)\tan\phi'\right]\sin(\theta_h+\beta)\,, \tag{30}$$

in which δ denotes the soil-wall friction angle.

Experimental investigations show that the earth pressure acting on a rigid retaining wall exhibits a nonlinear distribution commonly and a peak is found at lower 1/3 of the wall height. In present analysis, this finding is employed and the work rate of earth pressure can be derived as

$$W_{p_{ae}} = \omega P_{ae}f_1 = \omega P_{ae}\left\{\sin(\beta+\delta)\left(r_0\sin\theta_0 + \frac{2}{3}H\right) - \cos(\beta+\delta)\left(r_0\cos\theta_0 - r_h\cos\theta_h - \frac{1}{3}H\cot\beta\right)\right\}. \tag{31}$$

According to the kinematic limit analysis method, the energy balance equation can be formulated and the active earth pressure can be expressed as

$$P_{ae} = \frac{W_{\gamma'} + W_s^{ah} + W_s^{av} + W_Q + W_Q^{ah} + W_Q^{av} - D_c - D_{p_{ad}} - D_s^h - D_s^v}{\omega f_1}. \tag{32}$$

For convenient use in practice, an earth pressure coefficient K_{ae} is more popular. For unsaturated backfills, this coefficient can be written as

$$K_{ae} = \frac{P_{ae}}{h^2\sum_{i=1}^{m}\gamma_i'(m-i+0.5)}\,. \tag{33}$$

The maximum dynamic active earth pressure coefficient $K_{ae}(t)$ is generated when the backfill reaches a limit state. An optimization procedure was developed using the MATHEMATICA software.

3.4 Comparison with Published Results

For vertical cut slopes, Chen (1975) provided the stability factors of the slope using the kinematic limit analysis method, as shown in Table 1. As we all known, the slope reaches a limit state when the slope is characterized with this factor and the corresponding active earth pressure coefficient is zero. In present analysis, the

Table 1. Comparisons between the Solutions from Two Different Methods

	$\phi' = 10°$	$\phi' = 15°$	$\phi' = 20°$	$\phi' = 25°$	$\phi' = 30°$	$\phi' = 35°$	$\phi' = 40°$
$\gamma H/c$ in Chen (1975)	4.59	5.02	5.51	6.06	6.69	7.43	8.30
K_{ae} in this paper	0.0038	0.0025	0.0025	0.0018	0.0014	0.0015	0.0013

stability factor is employed and the K_{ae} is back calculated, as presented in the table. It can be found that, the K_{ae} in this paper are nearly equal to zero, indicating the reasonability of the proposed method. It should be underlined that not only for some relatively idealized conditions, some more complicated factors, such as the suction-related effects, the dynamic actions and the rainfall conditions can also be addressed satisfactorily using the proposed method.

4. Results

A steep unsaturated backfill restrained by rigid retaining wall is investigated. The parameters for slope configuration, mechanical and physical properties, seismic excitation and the SWCC are listed in Table 2.

4.1 Suction Effect

The dynamic change of the active earth pressure in a seismic period is studied. It can be found that, as shown in Fig. 4, the active earth pressure of unsaturated backfills presents sinusoidal variation and the peak emerges around 1/2 period of the seismic excitation. This is because that the sinusoidal assumption is used to simulate the seismic waves, resulting the sinusoidal variation of the inertial force and therefore the periodic variation of the slope stability.

Table 2. Parameters for Slope Configuration, Mechanical and Physical Properties, Seismic Excitation and the SWCC

Parameters for slope configuration	H	10 m
	β	90°
	z_0	2 m
	δ	10°
Parameters for mechanical and physical properties	c'	10 kPa
	ϕ'	20°
	γ_d	15 kN/m^3
	γ_{sat}	19.63 kN/m^3
Parameters for seismic excitation	G	25 MPa
	μ	0.3
	k_h	0.1
	k_v	0.05
	f_a	1.1
	T	0.2 s
	ζ	0
Parameters for SWCC (Curve B in Fig. 2)	q/k_s	0
	a_f	10 kPa
	n_f	2
	m_f	1
	ψ_r	100 kPa
	α	0.1 kPa^{-1}
	θ_r	0.076
Some related parameters	Q	10 kN/m
	m	60

The suction effect plays a significant role in the seismic active earth pressure estimations as shown in Fig. 4. It can be found that the earth pressure is overestimated significantly when the suction is ignored in the analysis. Furthermore, it is interesting to be noticed that the enhancement of soil suction to the earth pressure relates not only to soil types but also the seismic excitations. Evidently, the suction effect presents a sinusoidal variation as the seismic wave propagates. However, the variation of the suction effect is opposite with the seismic waves. The suction effect is significantly weakened (enhanced) when the seismic wave reaches the peak (valley). The suction effect on the seismic active earth pressure ranges from 15% – 32%. This is because that the inertia force varies during earthquakes and therefore the contribution of suction varies when the backfill reaches a limit state.

The internal friction angle, soil cohesion, surcharge load and soil-wall friction angle have significant on the suction effect, as shown in Fig. 5. As it is well known, the active earth pressure increases as the internal friction angle decreases and gets most pronounced when the backfill is under undrained conditions. The suction effect, however, increases as ϕ' increases, as shown in the graph. Similarly, the earth pressure increases while the suction effect declines with a decrease in soil cohesion. Furthermore, the suction effect vibrates significantly as the seismic wave propagates. In cohesionless backfills, the suction effect varies from only 4.5% to 12.1%. While for $c' = 20$ kPa, the suction effect varies from 37.4% to 100%. The suction effect relates to the surcharge

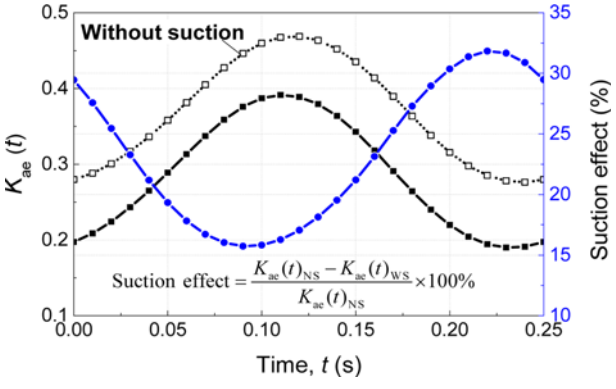

Fig. 4. Influence of Suction Effect on Active Earth Pressure (WS and NS denote with and without suction cases, respectively)

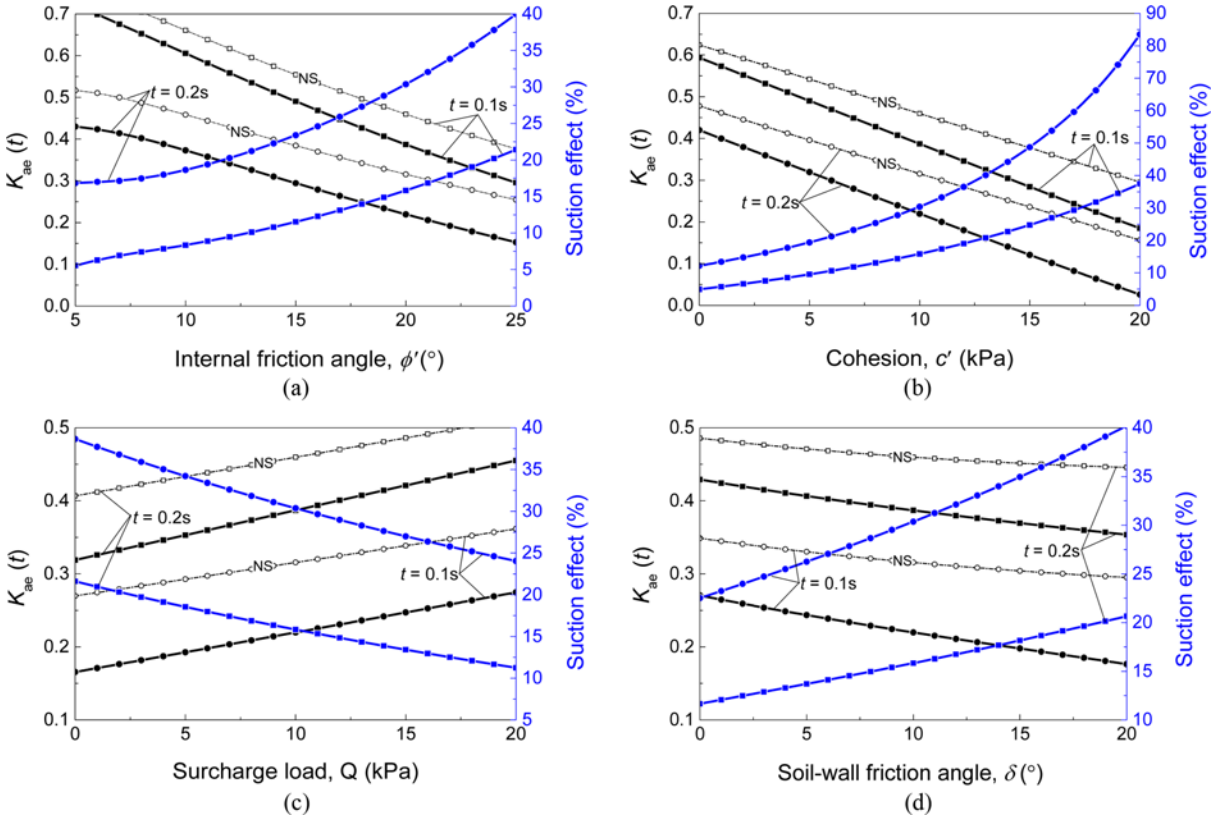

Fig. 5. The Active Earth Pressure and Suction Effect of Backfills with Different Values of: (a) Internal Friction Angle, (b) Soil Cohesion, (c) Surcharge Load, (d) Soil-Wall Friction Angle

load on the backfill surface as shown in Fig. 5(c). The contribution of suction to the backfill stability declines smoothly when the surcharge load increases. δ has prominent effect on the lateral earth pressures and depends on the seismic excitations. The influence of δ becomes relatively less evident when the seismic wave reaches the peak and relatively pronounced when the seismic wave reaches the valley.

4.2 Effect of Seismic Excitation Parameters

Figure 6 illustrates the influences of horizontal acceleration coefficient, vertical acceleration coefficient, amplification factor, soil shear modulus and seismic period on K_{ae} and the suction effect. The horizontal and vertical acceleration coefficients possess similar impacts on the seismic active earth pressure and the suction effect. The amplitude of K_{ae} increases rapidly as k_h and k_v increases. This is because that k_h and k_v denote the amplitude of the seismic acceleration, an increase in k_h and k_v leads to an increase in the seismic force and thereafter the earth pressure. The earth pressure relates closely to the peak of the seismic waves, while the suction effect relates closely the valley of the seismic waves.

The amplification factor has relatively small influence on the earth pressure and the suction effect, as illustrated in Fig. 6(c). Both the earth pressure and the suction effect increase as f_a increases. This is because that f_a determines the amplitude of the seismic waves. An increase in f_a results in an increase in the seismic force and finally the earth pressure. The soil shear modulus G determines the velocity of seismic waves in soils and hence the earth pressure and the suction effect, as indicated by Fig. 6(d). The amplitude of K_{ae} increases as soil shear modulus increases with the phase moving towards the negative direction. The amplitude of the suction effect remains identical and the phase moves towards the negative direction either. The seismic period influences the occurrence of the K_{ae} peak and the peak of the suction effect, as indicated by Fig. 6(e). The peak of K_{ae} increases slightly as T increase, while the peak of the suction effect remains nearly unchanged.

5. Conclusions

The seismic active earth pressure of unsaturated backfills was studied. According to the kinematic limit theorem, a horizontal slices method was suggested to formulate the energy balance equation. The upper bound solution to the seismic active earth pressure of the backfill was optimized. The roles of suction and seismic excitations in the earth pressure estimation were studied. The results indicate that:

1. The earth pressure is significantly overestimated when the suction effect is ignored. The suction effect depends not only on the soil type, but also relates closely to the seismic

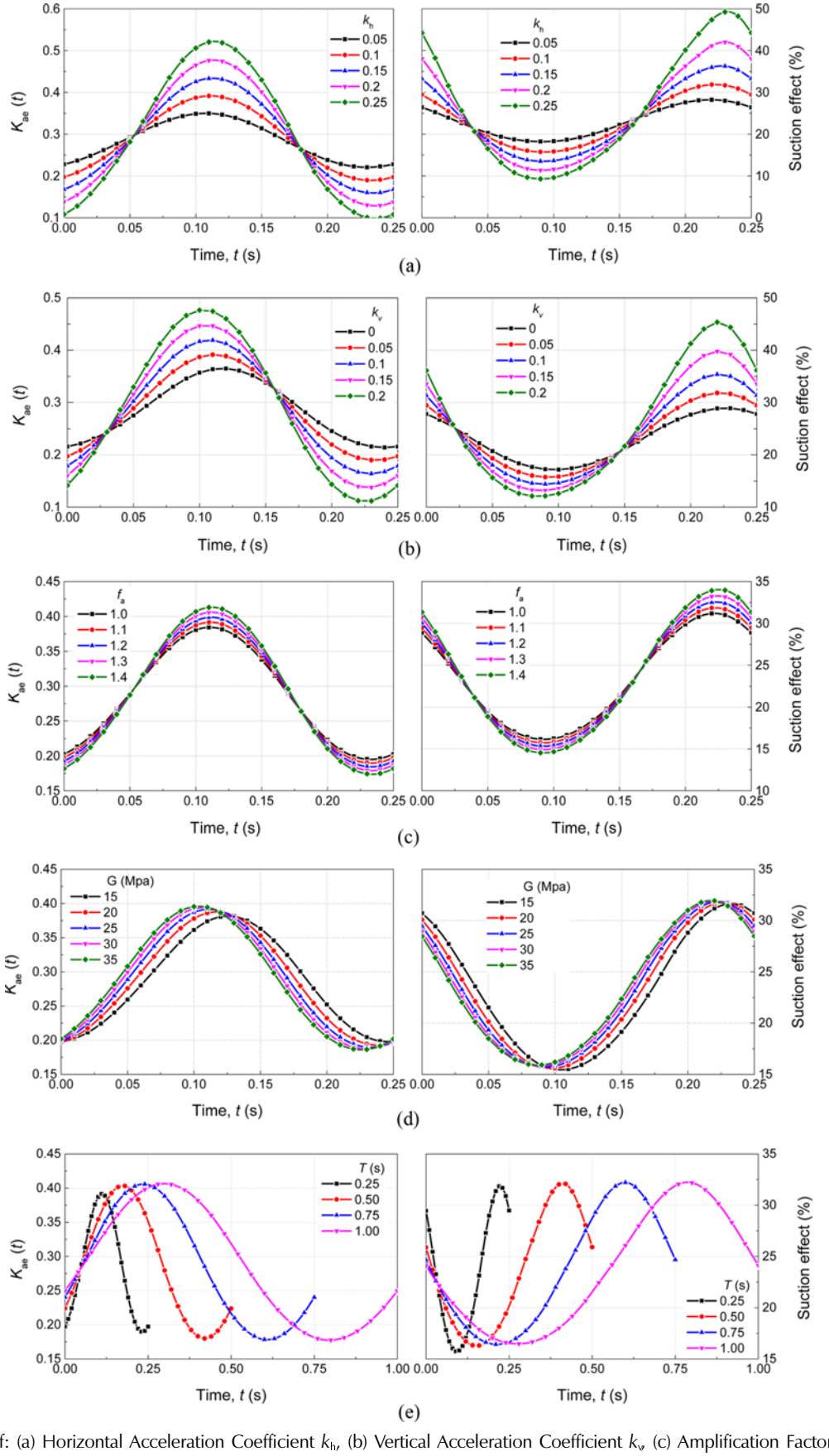

Fig. 6. Influence of: (a) Horizontal Acceleration Coefficient k_h, (b) Vertical Acceleration Coefficient k_v, (c) Amplification Factor f_a, (d) Soil Shear Modulus G, (e) Seismic Period T on the Active Earth Pressure Coefficient and the Suction Effect

excitations. Universally, the suction effect is weakened significantly when the seismic wave reaches the peak, and is enhanced when the seismic wave reaches the valley. The earth pressure increases while the suction effect declines with a decrease in soil friction angle, soil cohesion and soil-wall friction angle. The surcharge load possesses a converse influence on the earth pressure and the suction effect.

2. The horizontal and vertical seismic acceleration coefficients have a great influence on the active earth pressure. The earth pressure is more related to the peak of the seismic waves, while the suction effect relates more closely the valley of the seismic waves. The amplification factor has relatively small influence on the earth pressure and the suction effect. The amplitude of K_{ae} and the suction effect remains identical with the phase moving towards the negative direction as the soil shear modulus increases. The seismic period influences the occurrence of the K_{ae} peak and the peak of the suction effect. The peak of K_{ae} increases slightly as T increase, while the peak of the suction effect remains nearly unchanged.

Acknowledgments

This research was performed with the financial support from National Natural Science Foundation of China (Grant Nos. 52208345, 52008124, 52268054, 42272312), Opening Fund of State Key Laboratory of Geohazard Prevention and Geoenvironment Protection (Grant No. SKLGP2022K002), Natural Science Foundation of Jiangsu Province (Grant No. BK20210479) and the Fundamental Research Funds for the Central Universities (Grant No. JUSRP121055).

ORCID

Long Wang https://orcid.org/0000-0002-9117-0683
Lei Wang https://orcid.org/0000-0001-9423-7866
Junran Zhang https://orcid.org/0000-0002-4285-0746
Bo Chen https://orcid.org/0000-0001-9937-312X

References

Bishop AW (1959) The principle of effective stress. *Teknik Ukeblad* 106(39):859-863

Chen WF (1975) Limit analysis and soil plasticity. Amsterdam: Elsevier

Chen B, Gao Y, Sun DA, Li J (2021) Simple testing method for measuring the triaxial stress-strain relations of unsaturated soils at high suctions. *Geotechnical Testing Journal* 44(2):20190278, DOI: 10.1520/GTJ20190278

Chen B, Peng F, Zhang L, Sun DA (2023) Investigation on swelling characteristics of GMZ bentonite with different initial water contents. *Annals of Nuclear Energy* 181:109565, DOI: 10.1016/j.anucene.2022.109565

Choudhury D, Nimbalkar SS (2006) Pseudo-dynamic approach of seismic active earth pressure behind retaining wall. *Geotechnical and Geological Engineering* 24(5):1103-1113, DOI: 10.1007/s10706-005-1134-x

Fathipour H, Safardoost AH, Payan M, Veiskarami M, Chenari RJ (2021) Limit analysis of modified pseudodynamic lateral earth pressure in anisotropic frictional medium using finite-element and second-order cone programming. *International Journal of Geomechanics* 21(2): 04020258, DOI: 10.1061/(ASCE)GM.1943-5622.0001924

Fredlund DG, Morgenstern NR (1977) Stress state variables for unsaturated soils. *Journal of the Geotechnical Engineering Division* 103(5): 447-466, DOI: 10.1061/AJGEB6.0000423

Fredlund DG, Xing AQ (1994) Equations for the soil-water characteristic curve. *Canadian Geotechnical Journal* 31(4):521-532, DOI: 10.1139/t94-061

Hu W, Xu Q, McSaveney M, Huang RQ, Wang YJ, Chang CS, Gou HX, Zheng YS (2022) The intrinsic mobility of very dense grain flows. *Earth and Planetary Science Letters* 580:117389, DOI: 10.1016/j.epsl.2022.117389

Kokane AK, Sawant VA, Sahoo JP (2021) Novel pseudodynamic closedform solution for individual nail force in nailed vertical cut. *International Journal of Geosynthetics and Ground Engineering* 7(50):1-19, DOI: 10.1007/s40891-021-00294-7

Lei MF, Li J, Zhao CY, Shi CH, Yang WC, Deng E (2021) Pseudo-dynamic analysis of three-dimensional active earth pressures in cohesive backfills with cracks. *Soil Dynamics and Earthquake Engineering* 150(6):106917, DOI: 10.1016/j.soildyn.2021.106917

Liu M, Gorman DG (1995) Formulation of rayleigh damping and its extensions. *Computers and Structures* 57(2):277-285, DOI: 10.1016/0045-7949(94)00611-6

Lu N, Likos WJ (2004) Unsaturated soil mechanics. John Wiley and Sons, New York

Qin CB, Chian SC (2019) Pseudo-static/dynamic solutions of required reinforcement force for steep slopes using discretization-based kinematic analysis. *Journal of Rock Mechanics and Geotechnical Engineering* 11(2):75-85, DOI: 10.1016/j.jrmge.2018.10.002

Scaringi G, Hu W, Xu Q, Huang RQ (2018) Shear-rate-dependent behavior of clayey bimaterial interfaces at landslide stress levels. *Geophysical Research Letters* 45(2):766-777, DOI: 10.1002/2017GL076214

Steedman RS, Zeng X (1990) The influence of phase on the calculation of pseudo-static earth pressure on a retaining wall. *Geotechnique* 40(1):103-112, DOI: 10.1680/geot.1990.40.1.103

Sun DA, Wang L, Li L (2019) Stability of unsaturated soil slopes with cracks under steady infiltration conditions. *International Journal of Geomechanics*, 2019 19(6):04019044, DOI: 10.1061/(ASCE)GM.1943-5622.0001398

Vanapalli SK, Fredlund DG, Pufahl DE, Clifton AW (1996) Model for the prediction of shear strength with respect to soil suction. *Canadian Geotechnical Journal* 33(3):379-392, DOI: 10.1139/t96-060

Wang L, Hu W, Sun DA, Li L (2019) 3D stability of unsaturated soil slopes with tension cracks under steady infiltrations. *International Journal for Numerical and Analytical Methods in Geomechanics* 43(6):1184-1206, DOI: 10.1002/nag.2889

Wang L, Zhou AN, Xu YF, Xia XH (2022) Consolidation of partially saturated ground improved by impervious column inclusion: Governing equations and semi-analytical solutions. *Journal of Rock Mechanics and Geotechnical Engineering* 14(3):837-850, DOI: 10.1016/j.jrmge. 2021.09.017

Zeng X, Steedman RS (1993) On the behavior of quay walls in earthquakes. *Geotechnique* 43:417-431, DOI: 10.1680/geot.1994.44.3.557

Zhang YB, Chen FQ, Lin YJ, Chen HB (2022) Active earth pressure of narrow backfill against inverted t-type retaining walls rotating about the heel. *KSCE Journal of Civil Engineering* 26(4):1723-1739, DOI: 10.1007/s12205-022-1294-8

Zhang ZL, Yang XL (2021) Seismic stability analysis of slopes with cracks in unsaturated soils using pseudo-dynamic approach. *Transportation Geotechnics* 29:100583, DOI: 10.1016/j.trgeo.2021.100583

Zhou XY, He LQ, Sun DA (2022) Three-dimensional thermal modeling and dimensioning design in the nuclear waste repository. *International Journal for Numerical and Analytical Methods in Geomechanics* 46(4):779-797, DOI: 10.1002/nag.3321